universe

IMPACT FACTOR 2.5

CITESCORE 4.3

Review

Jet Precession in Gamma-Ray Bursts

Bao-Quan Huang and Tong Liu

Special Issue

New Insights into High-Energy Astrophysics, Galaxies, and Cosmology—Celebrating the 10th Anniversary of the Re-establishment of the Department of Astronomy at Xiamen University (2012–2022)

Edited by

Prof. Dr. Taotao Fang, Prof. Dr. Weimin Gu, Prof. Dr. Tong Liu and Prof. Dr. Beibei Liu

MDPI

https://doi.org/10.3390/universe10120438

universe

MDPI

Review

Jet Precession in Gamma-Ray Bursts

Bao-Quan Huang and Tong Liu *

Department of Astronomy, Xiamen University, Xiamen 361005, China
* Correspondence: tongliu@xmu.edu.cn

Abstract: Jet precession is thought to be a ubiquitous phenomenon in astronomical events of various scales, including gamma-ray bursts (GRBs). If GRB jets undergo precession, periodic features might be introduced into their light curves. Detecting these periodic signals is therefore crucial for confirming the properties of GRBs' central engines. However, periodic signals are always missing from observed GRB light curves. Against this backdrop, the broader effects of jet precession on GRBs have been widely studied. In this review, we summarize recent research progress on jet precession in GRBs. The main content focuses on four aspects of the effects of jet precession on GRBs: light curves, jet structures, polarization, and gravitational waves.

Keywords: gamma-ray bursts; gravitational waves; polarimetry; relativistic jets; shocks

1. Introduction

In high-energy astrophysics, jets refer to narrow beams of matter and energy with velocities close to the speed of light, and they are ubiquitous in astrophysical systems of various scales, such as active galactic nuclei (AGNs), X-ray binaries, and gamma-ray bursts (GRBs). Precession phenomena are expected to occur when there is misalignment between the direction of the launched jets and the angular momenta of part of these systems.

Jet precession in AGNs, including blazars [1–6], quasars [7–9], and radio galaxies [10,11], has been extensively studied over several decades. Observational evidence for the precession of AGN jets includes periodic signals in optical or radio light curves [12,13], periodic variations in the position angle of outflow components [14–18], and the S- or Z-shaped structures of large-scale radio jets [19–23], such as the clear S-shaped structure in the kpc-scale jets of the blazar 5BZU J1345+5332 [24]. There are several prevalent mechanisms driving jet precession in AGNs, including spin-induced precession [25–27], disk-driven precession [28,29], and Newtonian-driven precession [30–33]. Spin-induced and disk-driven precession are caused by the angular momenta of supermassive black holes (BHs) and their accretion disks, respectively, and both are mainly considered in single supermassive BH scenarios. Newtonian-driven precession arises from the rotation of an accompanying supermassive BH, and it is considered in binary supermassive BH scenarios. Spin-induced precession, also known as the Lense–Thirring precession effect [25], means that the frame drag caused by a rapidly rotating BH, such as a Kerr BH, can cause a particle to precess around the BH with its orbital plane inclined with respect to the equatorial plane of the BH. Thus, if the angular momentum directions of the BH and the disk are misaligned, the jets will precess. In addition, the Bardeen–Petterson effect is an extension of the Lense–Thirring effect [26] involving a viscous accretion disk, where regions of the disk corresponding to different radii are affected differently by the Lense–Thirring effect. Thus, under the Bardeen–Petterson effect, the disk is warped, resulting in three distinct regions: the inner, transition, and outer regions. The rotation axis of the inner region is aligned with the spin axis of the BH, while the outer region retains the original rotation direction. Continuous precession occurs in the transition region, since the rotation axis is misaligned with the spin axis of the BH. Regarding disk-driven precession, the precession of a jet ejected from the innermost disk can be driven by the massive outer disk because the angular momentum of

check for updates

Citation: Huang, B.-Q.; Liu, T. Jet Precession in Gamma-Ray Bursts. *Universe* **2024**, *10*, 438. https://doi.org/10.3390/universe10120438

Academic Editor: Alexandre Marcowith

Received: 22 October 2024
Revised: 19 November 2024
Accepted: 26 November 2024
Published: 27 November 2024

the massive outer disk greatly exceeds the total angular momentum of the inner disk and the central supermassive BH [28,29]. In Newtonian-driven precession, because the accretion disk around the primary BH is inclined to the orbital plane of the binary, the orbital motion of the companion BH can cause precession of the disk through dynamic torque, resulting in precession of the jet launched by the disk [30,31]. In such cases, the period of jet precession can reach thousands of years, which is usually used to explain the precession of large-scale (Kpc or Mpc) jets. However, the specific precession mechanism eventually needed to explain the precession phenomena in AGNs is determined not only by the precession period but also by multidimensional information.

In X-ray binaries, the strongest observational evidence for jet precession comes from the well-known SS433, whose jets change their orientation in space over a period of 162 days [34–36]. In addition, quasi-periodic oscillations (QPOs) observed in the emission are also well explained by jet precession [37,38], as seen in MAXI J1820+070 [39].

The observational and theoretical studies of AGNs and X-ray binaries have been explored in detail. Both involve BH accretion systems. Whether in AGNs or X-ray binaries, within the framework of BH accretion, jet precession mainly depends on the BH mass and spin, the accretion rate, and the type of accretion disk. Therefore, the mechanisms driving jet precession in these phenomena are intrinsically identical. Since GRBs can be induced by BH accretion systems, it is widely believed that GRB jets should also exhibit precession, with precession mechanisms analogous to those in AGN and X-ray binaries.

In GRBs, observational images of jet precession, like those of radio jets in AGNs, cannot be obtained due to the large distance, small scale, short duration, and precise period signals of jet precession, as observed in the X-ray binary SS433, have yet to be detected. Although convincing evidence has been consistently absent, GRB jet precession is universally expected.

GRBs are extremely energetic events in the Universe, characterized by a sudden and intense flash of gamma rays, releasing as much energy in a few seconds as the Sun will release in its entire 10 billion year lifetime, with a typical isotropic energy of about 10^{50}–10^{52} erg [40,41]. Based on the statistics of GRBs collected by the Burst and Transient Source Experiment (BATSE), GRBs are classified into short and long GRBs depending on whether or not their duration is greater than 2 s [42–44]. For a more physics-driven classification, GRBs can also be divided into Type I and II GRBs [45]. In general, short GRBs are thought to originate from the merging of compact objects [46], and the joint observation of GW170817/GRB 170817A has confirmed that binary neutron star (NS) mergers are the origin of short GRBs [47,48]. Long GRBs are thought to originate from the collapse of massive stars, and some have been found to be associated with supernova explosions [49]. Independent of the progenitors, there are two types of central engines: a rapidly rotating stellar-mass BH surrounded by an accretion disk [50] and a millisecond magnetar [51–53]. In a BH hyperaccretion scenario, the central engines can launch ultrarelativistic jets through neutrino annihilation [54] or Blandford–Znajek (BZ) [55] mechanisms. The emission of GRBs includes both prompt emission and afterglows. Prompt emission is generally thought to be caused by energy dissipation from ultrarelativistic jets. Prevalent models of energy dispersal include internal shock models [56–58], photosphere models [59,60], and magnetic reconnection models [61]. Afterglows are believed to originate from the interaction between the jets and the circumburst medium. For both, the dominant radiation mechanisms are considered to be leptonic models, i.e., synchrotron emission, synchrotron self-Compton emission, and the external Compton emission of accelerated electrons.

Jet precession can, in varying degrees, contribute to many aspects of GRBs, such as prompt (afterglow) light curves, jet structures, polarization, and gravitational waves (GWs). In this review, we summarize previous efforts to study jet precession in GRBs. In Section 2, the effects of jet precession on GRB light curves are presented. In Section 3, possible ejecta structures under jet precession are discussed. In Section 4, the properties of the polarization signal with jet precession are provided. In Section 5, the properties of GW signals under jet precession are presented. In Section 6, we give a brief summary.

2. Light Curves with Jet Precession in GRBs

2.1. Prompt Light Curves with Jet Precession

The light curves of GRB prompt emission are highly variable. Some show a single pulse with a rapid rise and exponential decay, while others show multiple pulses or complex multi-episode patterns separated by quiescent time. In addition, certain light curves exhibit a weak precursor component or extended emission. Periodic signals are considered convincing evidence of jet precession. However, early studies failed to identify high-quality periodic signals in prompt light curves [62–64]. This result implies the difficulty encountered by GRB jet precession in producing clear periodic signals, leading researchers to turn their attention to the search for QPOs. In recent years, several studies have been conducted to search for QPOs in the prompt emissions [65–68]. Chirenti et al. (2023) discovered kilohertz QPOs in the prompt emissions of short GRBs 910711 and 931101B using data from the BATSE archive [69]. Xiao et al. (2024) identified a potential QPO signal of approximately 22 Hz in the precursor emission of GRB 211211A [70], and a strong 19.5 Hz flux oscillation was also observed in this burst [71].

It is widely believed that the prompt emission of GRBs originates from the inner regions of the jets, and that jet precession may cause variations to be imprinted in the prompt light curves. Consequently, various jet precession models have been proposed to explain the diverse profiles observed in prompt light curves. Jet precession should essentially be driven by misalignment between the direction of the angular momentum of a BH and accretion matter. The accretion materials are derived from the companion star in short GRBs and from the envelopes of massive collapsars in long GRBs.

Regarding the scenario of binary systems or BH-NS mergers, Blackman et al. (1996) were the first to study a relativistic blob-emitting jet with precession primarily driven by Newtonian tidal torque in GRBs [72]. In their model, the precessing jet originates from a binary pulsar system, where the pulsars may be formed by the collapse of white dwarfs due to accretion. They used this precessing jet model to explain the short durations observed in GRBs, finding that the duration is mainly determined by the timescale during which the jet sweeps across the line of sight. Portegies Zwart et al. (1999) proposed that in a close NS-BH binary system, when the NS fills the Roche lobe of the BH, mass transfer from the NS to the BH occurs, leading to the formation of an accretion disk around the BH [73,74]. Misalignment between the binary angular momentum axis and the BH spin axis can result in a precessing jet, produced via the BZ mechanism. Their model also incorporated the nutation effect, which they applied in an attempt to reproduce the complex shapes of GRB prompt light curves. However, they later found that it was still difficult to explain some observed GRBs with asymmetric light curve shapes when only considering a precessing jet. As a result, they revised the model [75], proposing that a relativistic precessing jet interacts with the interstellar medium, producing a shock wave. The cooling of shock-accelerated electrons is then considered the cause of the asymmetric shapes in the prompt light curves, as well as of exponential decay in the emission flux. Using this modified model, they were able to fit the prompt light curves of several GRBs with reasonable precision. Stone et al. (2013) investigated jet precession in the context of short GRBs, focusing on a scenario where the accretion disk forms following an NS–BH merger [76]. They considered 10 different cases to explore how various disk parameters influence the precession period and number of precession cycles. They found that the precession period typically falls within the range of $\sim$0.01 to 0.1 s, while the precession angle is approximately 10°. Additionally, they found that the number of precession cycles is significantly influenced by disk viscosity, where higher viscosity leads to fewer precession cycles, which can further obscure the features of observed light curves. They suggested that these distinct precession characteristics could help differentiate between NS-NS mergers and NS–BH mergers as progenitors of short GRBs. Li et al. (2023) proposed a jet precession model within the framework of NS–BH mergers to predict possible QPOs in the prompt light curves of short GRBs [77]. In their model, the predicted QPOs primarily depend on several angular parameters, including the jet opening angle, viewing angle, and precession angle, with the periods ranging from

0.01 to 0.1 s. Additionally, due to the time required for the disk winds to align the jet with the disk, the QPOs may appear with a delay relative to the trigger time. They suggested that the delayed QPOs are a characteristic feature of NS–BH mergers with misaligned orbital planes.

Regarding BH accretion systems in which progenitors are not considered, Reynoso et al. (2006) investigated spin-induced precession and nutation occurring in a neutrino-cooled disk around a stellar-mass Kerr BH in the framework of GRBs [78]. In their model, the precession and nutation of the disk are transferred to relativistic jets launched via the BZ mechanism. The combination of these effects can explain the oscillating microstructures of the prompt light curves, as well as the shape of a slow rise and fast decay observed in some GRBs. Lei et al. (2007) proposed a precessing jet model that incorporates magnetic coupling processes, accounting for the evolution of the half-opening angle of the magnetic flux on the BH horizon [79]. They found that the model can produce a light curve profile characterized by a fast rise and slow decay. Liu et al. (2010) proposed a model of jet precession driven by a neutrino-dominated accretion disk to explain the prompt light curves of GRBs [80]. In their model, a critical radius is defined where the angular momentum of the BH equals that of the disk. Within this radius, the rotation of the inner disk aligns with the spin direction of the BH, while beyond this radius, the outer disk retains its original rotation. Since the angular momentum of the outer disk is significantly larger than the combined angular momentum of the inner disk and the BH, the outer disk drives the precession of both the inner disk and the BH, resulting in jet precession. The characteristics of the precessing jet depend on the BH mass $M_{\rm BH}$, accretion rate $\dot{M}$, and spin parameter a. This model not only provides a potential explanation for the temporal evolution of GRB pulses but also demonstrates that the spectral peak energy $E_{\rm p}$ tracks the flux evolution under jet precession.

These jet precession models were used to explain the characteristics of the prompt light curves of certain GRBs. Wang et al. (2022) proposed that GRB 200826A should be a long GRB resulting from the collapse of a massive star, with the prompt emission consisting of both precursor and main emissions [81]. They interpreted the observed prompt emission, lasting approximately 1 s, as being the precursor emission, and concluded that the main emission was not detected. They attributed this absence to jet precession, which likely caused the radiation region to shift away from the line of sight of the observers. Gao et al. (2023) suggested that the repeating episodes with similar temporal profiles observed in the prompt light curves of some GRBs, such as GRB 950830, could be explained by a precessing jet [82]. Li et al. (2023) attributed the delayed QPO behavior in the prompt light curve of short GRB 130310A to the precession jet from an NS-BH merger [77]. Zhang et al. (2023) used the jet precession and nutation model in [73] to explain three emission episodes in the prompt light curve of GRB 220408B, which exhibited similar temporal and spectral characteristics [83]. They obtained values for the precession and nutation periods of GRB 220408B, 18.4 ± 0.2 s and 11.1 ± 0.2 s.

Overall, although the jet precession model has been employed to explain the complex behavior of prompt light curves, convincingly observational evidence supporting GRB jet precession, namely significantly periodic signals, is always missing, and QPOs are an alternative being considered. A possible reason for the absence of significant periodic signals is that most observed GRBs are viewed nearly on axis, and the precession angle is quite small when their jets are precessing. As a result, the effects of jet precession are weakly reflected in the prompt light curves. Of course, precession should occur in GRBs during their violent evolution. GRBs are catastrophic events, and during the early phases, the central engines might experience instabilities due to irregular accretion, leading to significant and irregular variations in both the precession period and angle as well as in jet luminosity.

2.2. Afterglow Light Curves with Jet Precession

In general, prompt gamma-ray emission is followed by long-lasting (hours to days) multi-band afterglow emission, ranging from radio to X-ray [84], sometimes also accompanied by high-energy and very high-energy photons (>100 GeV), as seen in GRB 221009A, with detected photon energies of up to 5 TeV [85]. Since the first afterglow event was discovered in 1997 (GRB 970228) [86], GRB afterglow has been extensively studied. Multi-wavelength afterglow is believed to be produced by electrons accelerated by the shock waves generated as ultrarelativistic jets sweep up the circumburst medium, according to the external shock model [84,87]. In the Swift era, a large number of X-ray afterglow events are observed, and the shapes of the X-ray light curves exhibit diversity. These can be categorized into five segments: rapid decay, flat decay or plateau, normal decay, jet break, and one or more flares [88]. These five phases are thought to have different physical origins, with fast-decaying phases having the same origin as the prompt emission. Flat decay (plateaus) may be due to energy injection from the central engines. Normal decay with a power-law index is in agreement with the prediction of the standard external shock model. Jet break occurs when the visible region is larger than the physical region of the jets. Some flares are thought to be likely associated with the activation of the central engines. A proposition of current relevance, regarding the shape of the X-ray light curve, is the idea that most shallow decay (plateaus) and flares share the same physical origin [89], though the origin of the plateaus is still under debate.

Jet precession can affect not only prompt light curves but also afterglow light curves. One possible effect is the emergence of QPO behavior in the afterglow light curves. Currently, significant effort has been dedicated to searching and studying the behavior. One view is that QPOs in the afterglow light curves originated from precessing millisecond magnetars. In cases where the central engine of a GRB is a rapidly rotating and highly elliptical millisecond magnetar, Suvorov and Kokkotas (2020) proposed that its early precession could cause QPOs of spin-down luminosity, which should manifest as QPO signals in the plateau phase of X-ray afterglow light curves [90]. To test this, they analyzed two GRBs with plausible QPOs in X-ray plateaus likely driven by millisecond magnetars: long GRB 080602 and short GRB 090510. They fitted the X-ray afterglow light curves of these bursts using two models: one for a non-precessing millisecond magnetar and another for a precessing one. Using the Akaike Information Criterion, they found that the precessing millisecond magnetar model provided a better fit to the data. As a result, they suggested that QPOs in the X-ray afterglow plateaus of GRBs 080602 and 090510 could be evidence of precession in a newly formed millisecond magnetar. They further explored whether this precession is a common phenomenon among newborn millisecond magnetars by expanding the number of sample GRBs, selecting 25 short GRBs. They applied the same method to fit these GRBs, finding that 16 out of the 25 GRBs favored the precessing millisecond magnetar model, representing 64% of the sample [91]. Zou et al. (2021) analyzed GRB 101225A and found plausible QPOs in its X-ray afterglow light curve between 4900 s and 7500 s, with periods of 488 s and 250–300 s, at a confidence level of 90% [92]. They applied a magnetar precession model to explain these QPOs and found that, when accounting for spin-down dominated by GW radiation, the signals can be well explained. In addition to GRB 101225A, they also found candidate QPOs in GRB 180620A with a period of approximately 650 s [93] and in GRB 210514A with a period of approximately 11 s [94], which they explained using the magnetar precession model. Besides the scenario of precessing millisecond magnetars, a rapidly spinning and precessing BH could also serve as another scenario for QPOs. Zheng et al. (2024) proposed that QPOs observed during plateau and subsequent sharp decay phases can be produced by a precessing BZ jet [95]. Using this model, they explained the oscillations appearing in the plateau and steep decay phases of X-ray afterglow light curves of GRB 050904. They suggested that the simultaneous emergence of QPOs in plateau and steep decay phases could serve as a potential clue for the central engines as a BH, rather than a millisecond magnetar.

In addition to QPOs, other special features of jet precession may also manifest in X-ray afterglow light curves, such as evolving flares, multiple peaks with distinct profiles, and plateaus. Hou et al. (2014) used the jet precession model proposed by Liu et al. (2010) [80] to explain the origin and evolution of flares appearing in the afterglow phase of GRB 130925A [96]. GRB 130925A was jointly detected by Swift, Fermi, Konus–Wind, and INTEGRAL, with observations revealing multiple X-ray flares that exhibited noticeable temporal evolution. They found that the time intervals between adjacent flares positively correlated with observation time, which can be interpreted as the evolution of the jet precession period. Based on the observed flare and within the framework of the precessing jet, they suggested that the central engine of GRB 130925A involved a rapidly spinning BH formed from the collapse of a massive star, and provided rough estimates of the BH mass and spin. The same model was also employed to account for the potential periodic signals of approximately 86 s in the X-ray bump of GRB 121027A [97]. Li et al. (2023) investigated afterglow light curves with the jets possessing asymmetric structures potentially caused by jet precession [98]. In their model, the resulting ejecta were divided into several regions with different velocities and energies. The combined contributions of these regions produced afterglow light curves characterized by multiple peaks with distinct profiles.

Huang and Liu (2021) investigated the impact of long-lasting jet precession on X-ray afterglow light curves and found that the precession leads to the appearance of a plateau without QPO signals in the afterglow light curves under a reasonable range of parameters [99]. As shown in Figure 1, they approximated the precession process as the result of discrete sub-jets continuously filling in along the precessing helical path (blue curve). The angle between the Z-axis and the jet axis is defined as the precession angle $\theta_{\rm pre}$, while the angle between the Z-axis and the line of sight is defined as the viewing angle $\theta_{\rm obs}$. The half-opening angle of the jet is denoted as $\theta_{\rm jet}$. The number of discrete sub-jets depends on the precession angle $\theta_{\rm pre}$ and the angle between the axis of adjacent sub-jets. In the first precession cycle, the sub-jets interact with the circumburst medium, producing external forward shock waves. As the shock waves sweep through the medium, they slow down after accumulating a certain amount of the medium. The sub-jets from subsequent precession cycles catch up with the decelerated forward shock waves, resulting in energy injection.

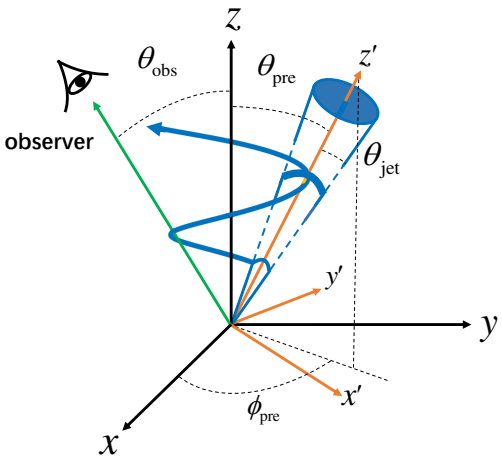

Figure 1. A cartoon depiction of a GRB precessing jet (adapted from [99]).

Under this physical picture, the evolution of the Lorentz factors Γ of the forward shock waves affected by the jet precession can be described as follows [100]:

$$\frac{d\Gamma}{dt} = -\frac{\Gamma(\Gamma^2-1)(\hat{\gamma}\Gamma-\hat{\gamma}+1)c^2\frac{dm}{dt} - \Gamma(\hat{\gamma}-1)(\hat{\gamma}\Gamma^2-\hat{\gamma}+1)(3u/R)\frac{dR}{dt} - \Gamma^2\frac{dE_{\rm inj}}{dt}}{\Gamma^2(M_0+m)c^2 + (\hat{\gamma}^2\Gamma^2-\hat{\gamma}^2+3\hat{\gamma}-2)u}, \quad (1)$$

where $E_{\rm inj}$ represents the energy injected as the sub-jets catch up with the forward shock waves, M_0 denotes the initial mass, R is the distance from the central source, u refers to the internal energy, m is the sweep-up mass from the circumburst medium, t is the time measured in the observer frame, c denotes the speed of light, and $\hat{\gamma}$ is the adiabatic index. In addition, energy injection term $dE_{\rm inj}/dt$ is written as [99]

$$\frac{dE_{\rm inj}}{dt} = \begin{cases} P_{\rm jet}, & T_{\rm start} < t < T_{\rm end}, \\ 0, & \text{others}, \end{cases} \tag{2}$$

where $T_{\rm start} = ((i-1)\Delta t + j\tau)$, $T_{\rm end} = (i\Delta t + j\tau)$, $i\ (= 1, 2, \ldots, k)$ refers to the sequence number of sub-jets within each precession period, $j\ (= 1, 2, \ldots, t_{\rm end}/\tau - 1)$ represents the serial number of precession cycles, τ is the precession period, and $\Delta t = \tau/k$. $P_{\rm jet}$ represents the jet power.

In their model, synchrotron radiation is produced by shock-accelerated electrons. To accurately compute the radiation flux from the forward shock waves, each shock wave generated by the sub-jets interacting with the circumburst medium during the first precession cycle is divided into 300×1000 emitters along the θ' and ϕ' directions in the spherical coordinates comoving with the precessing jet, while the corresponding comoving Cartesian coordinates are denoted as (x', y', z'), with the z' axis aligned along the jet axis (as shown in Figure 1). In addition, due to the line-of-sight effect, radiation photons from regions moving in directions not directly aligned with the line of sight will experience a time delay, compared with photons emitted from regions moving directly toward the line of sight. This can be expressed as $t_{\rm de} = R(1 - \cos\theta_{\rm em})/c$, where $\theta_{\rm em}$ represents the angle between the radiation emitters and the line of sight. Finally, the total observed flux from a precessing GRB jet is obtained by summing the flux from radiation emitters that have the same observation time.

First, the case of the precession jet without power evolution was explored. Figure 2 presents the X-ray afterglow light curves for a precessing jet with steady power. It is evident that plateaus appear in a large portion of the light curves, some of which display slight positive slopes. In this figure, the influence of various parameters on the plateaus is examined, including the precession period τ, precession angle $\theta_{\rm pre}$, jet power $P_{\rm jet}$, and viewing angle $\theta_{\rm obs}$. The left and right columns of the figure show the results for $\tau = 10\,{\rm s}$ and $100\,{\rm s}$, respectively. Clearly, plateaus with shorter precession periods appear earlier (left column). Additionally, there is little difference between plateaus at $\theta_{\rm pre} = 5^\circ$ and 10°, but the fluxes of the plateaus with $P_{\rm jet} = 10^{49}\,{\rm erg\,s^{-1}}$ are approximately an order of magnitude lower than those with $P_{\rm jet} = 10^{50}\,{\rm erg\,s^{-1}}$. The viewing angle also significantly affects the plateaus. When the line of sight is outside the precession path, the plateaus vanish, and a bump-like feature with a relatively lower flux emerges at a later time. Mainstream models for the origin of the plateaus involve energy injection. The findings imply that jet precession could be a new mechanism for energy injection.

Overall, QPOs seem to appear more easily in the X-ray afterglow light curves (several hundred to thousands of seconds) than in the prompt light curves. However, the potential QPO signals in the X-ray afterglow light curves have relatively poor quality. Hopefully, future instrumentation will detect more QPOs of higher quality, such as the Transient High-Energy Sky and Early Universe Surveyor (THESEUS). On the other hand, jet precession could also leave traces in the X-ray afterglow light curves through other features, such as a plateau structure, whose origin remains controversial. Additionally, if the late-time flares are caused by jet precession, they should be preceded by similar flares with higher peak fluxes, and evidence of approximately regular evolution should be observed in the time intervals between adjacent flares. In this context, evidence from multiple wavebands should be considered when testing for jet precession by GRB afterglow light curves.

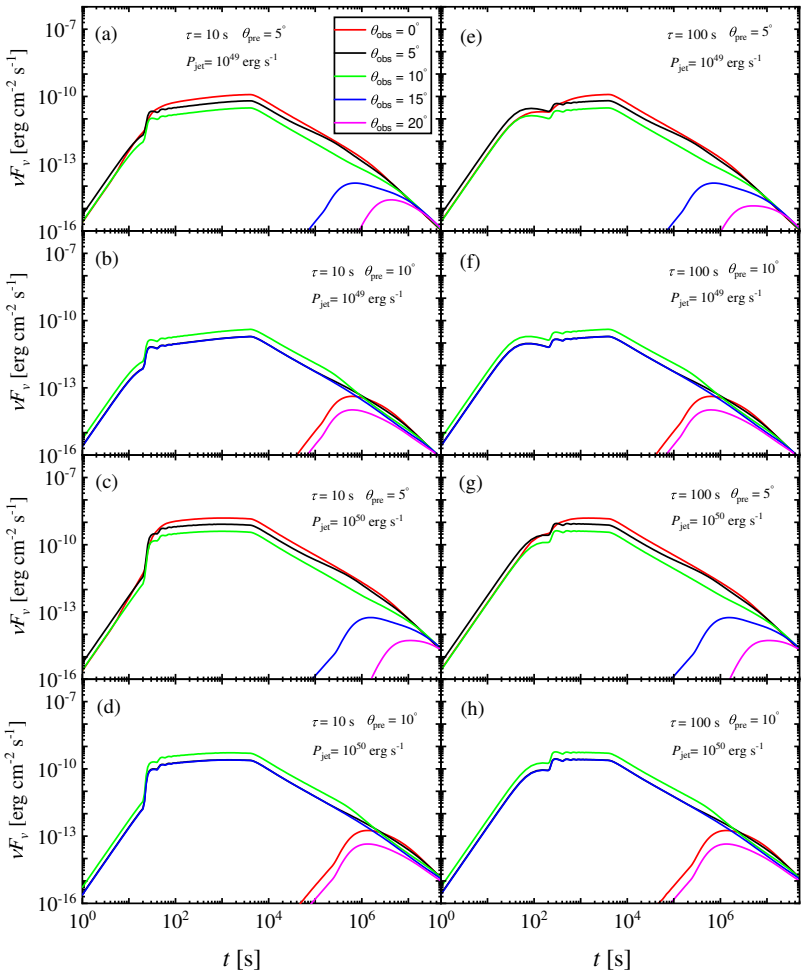

Figure 2. X-ray afterglow light curves of a precessing jet with steady power. The precession periods $\tau = 10\,\mathrm{s}$, $100\,\mathrm{s}$, the precession angles $\theta_{\rm pre} = 5^\circ$, 10°, and the initial jet powers $P_{\rm jet} = 10^{49}\,\mathrm{erg\,s^{-1}}$, $10^{50}\,\mathrm{erg\,s^{-1}}$ are adopted. The red, black, green, blue, and magenta lines represent the light curves for $\theta_{\rm obs} = 0^\circ$, 5°, 10°, 15°, and 20°, respectively (adapted from [99]).

3. Ejecta Structures with Jet Precession in GRBs

The structure of a jet might be either uniform [101] or structured [102]. In a uniform jet, often referred to as a "top-hat" jet, the energy per unit solid angle remains constant regardless of the angular distance from the jet axis, exhibiting sharp cutoffs at the edges. In contrast, structured jets exhibit variations in both energy density and Lorentz factors with angular distance. The most common models of structured jets include power-law [103–105] and Gaussian [106,107] structured jets. Although structured jets have been proposed for a long time and used to explain certain light curve features, such as double jet breaks and X-ray flares [106–109], their physical origin remains unclear. For a long time, research on structured jets was limited because the top-hat jet model was sufficient for explaining most observed GRBs. This situation changed with successful detection of the multi-wavelength afterglow of GRB 170817A, associated with GW170817 [47,48,110], which indicated that its jet was consistent with a structured jet [111,112]. The physical origin of structured jets has gained renewed attention. The structures of GRB jets determine the morphology of light curves and provide rich information about their formation and propagation. These structures are influenced by several factors, including the properties of the central compact object, the characteristics of the accretion disk, and the nature of the stellar envelope (in the case of massive star collapse) or ejecta (in the case of binary compact object mergers). Numerical simulations suggest that as a jet propagates through a dense envelope, its structure can be reshaped by interaction with the medium and thus differ significantly

from its initial structure after breakout [113–115]. Additionally, as the jet passes through the envelope, it can heat the surrounding material, forming a hot cocoon [116]. If this cocoon breaks out alongside the jet, it can create a composite structure, which may be one possible origin of structured jets. Structured jets may be either inherent from the central engines or gradually shaped by external factors. Although the structured jets formed by cocoons are fundamentally different from those caused by jet precession, it is difficult to distinguish them through existing observations. The cocoon characteristics critically depend on the interaction between the jets and the progenitor's envelope or the ejecta, and even depend on the circumstances. If the structures of the envelope or the ejecta can be constrained using other observations, then the characteristics of the cocoon may be narrowed down and the origin of the structured jet can be identified.

Huang et al. (2019) investigated the structure of a short-duration precessing jet during the afterglow phase and found that jet precession causes a top-hat jet to exhibit structured profiles [117]. In their calculations, they divided the precession duration of the top-hat jet into multiple equal and sufficiently short time intervals. Thus, the energy emitted by the jet during each interval is the product of the jet power and the interval duration. The ejecta during each interval were discretized into a large number of cells, each carrying energy equal to the total energy emitted in that interval divided by the number of cells. They further divided the plane perpendicular to the jet precession axis into fine grids and projected all cells emitted in each time interval onto this plane. By tracking the number of cells within each grid and calculating the total energy carried by them, they derived the energy distribution of the jet on the plane perpendicular to the precession axis, as illustrated in Figure 3.

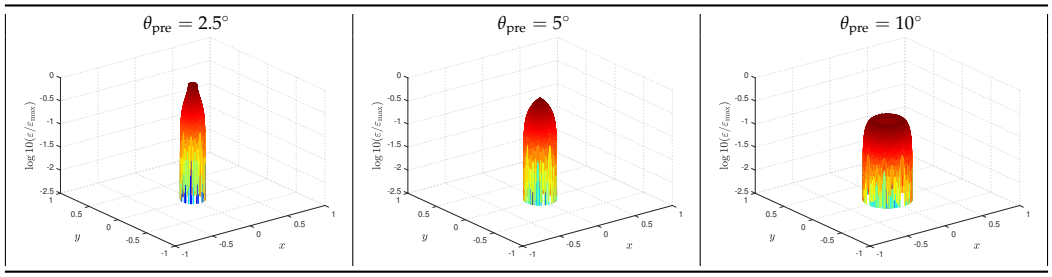

Figure 3. Distribution of energy density of a precessing GRB jet with a constant power, considering precession angles $\theta_{\rm pre} = 2.5^\circ$, 5°, and 10° (adapted from [117]).

Figure 3 shows the distribution of energy density ε with different precession angles, where the left, middle, and right panels represent the results for the precession angles $\theta_{\rm pre} = 2.5^\circ$, 5°, and 10°, respectively. The distribution of energy density is projected in the x-y plane with $x = \sin\theta\cos\phi$ and $y = \sin\theta\sin\phi$. Since the half-opening angle of the jet is set, $\theta_{\rm jet} = 5^\circ$, then $\theta_{\rm pre} = 2.5^\circ$, 5°, and 10° correspond to cases of $\theta_{\rm pre} < \theta_{\rm jet}$ (case I), $\theta_{\rm pre} = \theta_{\rm jet}$ (case II), and $\theta_{\rm pre} > \theta_{\rm jet}$ (case III), respectively. In case I, when $\theta < \theta_{\rm jet} - \theta_{\rm pre}$, ε remains constant over θ; however, when $\theta > \theta_{\rm jet} - \theta_{\rm pre}$, ε exhibits power-law decay with a sharp cutoff tail. This structure can be described as [104,117]

$$\frac{\varepsilon(\theta)}{\varepsilon_{\rm max}} = \begin{cases} 1, & \theta \le \theta_{\rm c}, \\ \left(\frac{\theta}{\theta_{\rm c}}\right)^{-k_1}, & \theta_{\rm c} < \theta \le \theta_{\rm m}, \\ \left(\frac{\theta_{\rm m}}{\theta_{\rm c}}\right)^{-k_1} \exp\left[\frac{-(\theta-\theta_0)^2}{2\theta_{\rm g}^2}\right], & \theta_{\rm m} < \theta < \theta_{\rm pre} + \theta_{\rm jet}, \end{cases} \tag{3}$$

where $\theta_{\rm c} = 2.5^\circ$, $\theta_{\rm m} = 5^\circ$, $k_1 = 1.05$, $\theta_0 = 4.8^\circ$, and $\theta_{\rm g} = 1.6^\circ$. In case II, ε can be well described by the Gaussian function [106,117]

$$\varepsilon(\theta) \propto \exp[-(\theta - \theta_l)^2/2\theta_{\rm n}^2], \tag{4}$$

where $\theta_l = 1.6^\circ$ and $\theta_{\rm n} = 5.0^\circ$. In case III, both power-law and Gaussian function cannot adequately describe ε evolving over θ. In this case, the jet in the afterglow phase presents

a ring shape. The results from Figure 3 indicate that the jet structures are significantly dependent on the jet precession angle under jet precession. The jet structures will be significantly more complex if the power evolution of the precessing jet is considered, as shown in Figure 4 of the paper.

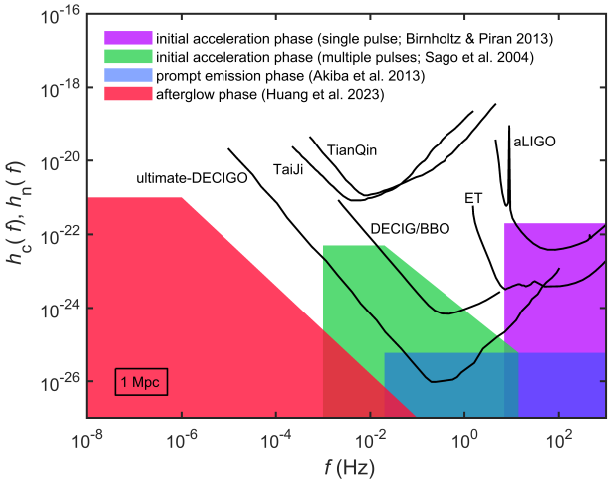

Figure 4. The characteristic amplitude ranges of GW signals from GRB jets at various stages, assuming a distance of 1 Mpc. The shaded areas in purple, green, blue, and red indicate the initial acceleration phase (single pulse) [118], initial acceleration phase (multiple pulses) [119], prompt emission phase [120], and afterglow phase [121], respectively. The black curves represent the sensitivity thresholds of various detectors, including aLIGO, ET, TianQin, Taiji, DECIGO/BBO, and ultimate-DECIGO (adapted from [121]).

4. Polarization Signal with Jet Precession in GRBs

The polarization signals of GRB emission primarily arise from the ordered nature of magnetic fields, which offer insights into the magnetic field characteristics of the emission region. Therefore, polarization detection is regarded as a unique tool for studying the characteristics of magnetic fields in GRB jets. In polarization measurements of the prompt emission phase, the detected signals typically exhibit high polarization degrees (PDs $>$ 50%) [122–125]. Since prompt emission arises from internal energy dissipation within the jet, high PDs are believed to result from large-scale ordered magnetic fields associated with GRB central engines. Additionally, a 90° reversal of polarization angles (PAs) within a single pulse has also been observed [126]. In afterglow polarization detection, the focus primarily lies in the optical band, which is divided into early and late optical afterglow polarization measurements. Early optical afterglow polarization measurements typically exhibit PDs mainly in the range of 3–30% [127–134], whereas those in late optical afterglows generally remain below 3% [135–142]. The polarization levels measured in late optical afterglow are consistent with the expectations for a forward shock origin. However, most PDs measured in early optical afterglows do not match the high polarization levels predicted for reverse shock waves with large-scale ordered magnetic fields [143], falling significantly below theoretical expectations.

The polarization behavior of GRB emission may be affected by GRB jet precession. Lan et al. (2019) studied the polarization characteristics of several astrophysical phenomena, including GRBs, in the context of jet precession [144]. Their research demonstrated that GRB jet precession can result in periodic signals in the polarization curves of prompt gamma-ray emission, with the polarization angle undergoing sudden 90-degree flips. They suggested that these polarization features could potentially serve as a key factor in identifying jet precession. Huang et al. (2022) investigated the impact of long-lasting jet precession on the polarization signals of early optical afterglow and found that jet precession can lead to a certain degree of depolarization [145]. To model the precession and calculate the polarization signals of the early optical afterglow, they adopted the jet

dissociation model proposed by [99]. In the model, the interaction of each sub-jet with the circumburst medium during the first precession cycle gives rise to the formation of a pair of shocks: a forward shock wave moving outward through the circumburst medium and a reverse shock wave propagating inward through the jet material, with the dynamics of both shock waves determined by solving a set of differential equations. In addition, large-scale ordered magnetic fields are considered within the jet, with two configurations explored: a toroidal magnetic field and an aligned magnetic field. Additionally, they assumed that no large-scale ordered magnetic fields exist in the circumburst medium. Thus, only randomly amplified magnetic fields are present downstream of the forward shock waves, and high polarization signals in the early optical afterglow are primarily generated by radiation from the reverse shock waves. Further, to quantify the overall polarization effect, they summed the Stokes parameters from each forward–reverse shock system at the same observation time. However, before summing, it was necessary to transform the Stokes parameters from the coordinate system comoving with jets to a global coordinate system [144].

Figure 5 shows the light curves and polarization signals of early optical afterglows dominated by reverse shock waves under jet precession, with the left and right panels corresponding to the field configurations being aligned and toroidally magnetic, respectively. Different colored lines represent the results for different $\theta_{\rm obs}$, with $\theta_{\rm obs}$ being the angle between the line of sight and the precession axis. The top, middle, and bottom panels show the light curves and the evolution of PDs and PAs over time, respectively. In the top panel, the light curves are seen to broadly remain consistent across different magnetic field configurations, implying that the magnetic field configurations do not significantly affect the light curves. In the middle panel, the PD in $\theta_{\rm obs} = 0^\circ$ is almost zero, indicating that the high PDs produced in the reverse shock waves with large-scale magnetic fields can almost be canceled out by the precession process. However, this is strongly dependent on $\theta_{\rm obs}$, and as $\theta_{\rm obs}$ increases, the depolarization effect caused by jet precession becomes insignificant. In other word, it becomes evident only when the line of sight is around the precession axis. In the bottom panel, the evolution of PAs over time exhibits several features, including periods of basic constancy, gradual decay, and abrupt changes. The PA characteristics are determined by the magnetic field directions in the visible core. For example, the near-constant PA with time in $\theta_{\rm obs} = 7^\circ$ implies that the ordered magnetic field in the visible core has a stable direction. However, when the Lorentz factor of the jets decreases, the observational region increases, and the sub-jets moving at different positions become observable such that the direction of magnetic fields in the observable core may abruptly or gradually change, as reflected in the PA evolution.

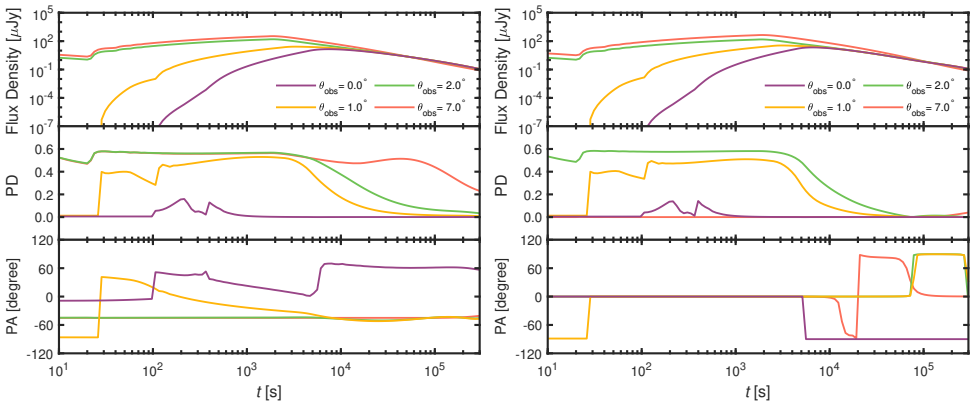

Figure 5. Light curves and polarization evolution of early optical afterglow dominated by reverse shock waves. The left and right panels are the results of magnetic field configurations in the reverse shock waves being aligned and toroidal, respectively. The top, middle, and bottom panels show the light curves and the time evolutions of polarization degrees and polarization angles, respectively. The violet, yellow, green, and red lines represent the results with observation angle $\theta_{\rm obs} = 0^\circ$, 1°, 2°, and 7°, respectively (adapted from [145]).

In order to test the possibility that this model could explain the generally low PDs measured in the early optical afterglows, they collected GRBs with PD measurements within the early optical afterglow phase ($<10^3$ s), and a sample of 16 GRBs was obtained where seven GRBs (GRBs 090102, 091208B, 101112A, 110205A, 120308A, 141220A, and 190114C) had a definite PD value and the others only had an upper limit of PD. They matched the PDs of these GRBs with the theoretical results for different $\theta_{\rm obs}$, finding that the measured PDs significantly support a small angle of $\theta_{\rm obs}$. Then, they examined the effects of other relative parameters on the PDs, including the precession period of the jets, duration of the jets, initial Lorentz factor, jet luminosity, magnetization parameter, fraction of internal energy density downstream of the reverse shock waves shared by the electrons, and redshift. It was found that these parameters do not significantly impact the PDs compared to $\theta_{\rm obs}$. This indicates that jet precession is a potential origin of the low PDs observed in early optical afterglow. However, due to the lack of direct observational evidence for jet precession, it remains impossible to attribute the low polarization degree of any GRB in the sample to jet precession.

5. GW Signal with Jet Precession in GRBs

The successful detection of GW150914 in 2015 marked the beginning of a new era in GW detection [146]. In 2017, the joint observation of GW170817 and GRB 170817A signaled the start of a new era in multimessenger astronomy [47,48]. In addition to the mergers between binary compact objects, known as strong GW sources, the ultrarelativistic jets of GRBs could also be potential sources of strong GWs. The GW signals from GRB jets have been studied extensively and are produced by the acceleration of the jets [118–120,147], independent of the energy form, known as the GW memory. If the jet interacts with a dense stellar envelope or ejecta, this GW memory can be modulated [148]. Similarly, the GW memory can be affected during the afterglow phase if energy is injected from reactivation of the central engines [121]. Figure 4 illustrates the GWs of GRB jets at different stages. The shaded areas in purple, green, blue, and red indicate the initial acceleration phase (single pulse) [118], initial acceleration phase (multiple pulses) [119], prompt emission phase [120], and afterglow phase [121], respectively. In the initial acceleration phase, the amplitude and frequency range of GWs are larger and narrower, respectively, in the case of a single-pulse scenario than in a multiple-pulse scenario. In the prompt emission phase, the frequency of GWs is slightly lower than that in the initial acceleration phase. When the source position is 1 Mpc, they have the potential to be detected by the Ultimate Decihertz Interferometer Gravitational Wave Observatory (Ultimate-DECIGO). Furthermore, the signal from the afterglow phase exhibits a markedly lower frequency range in comparison to that in the acceleration and prompt phases. Romero et al. (2010) studied the GWs produced by a precession system that includes a neutrino-cooled accretion disk in GRBs [149]. They assumed that the precession is driven by a spin-induced mechanism and discussed scenarios of both long and short GRBs. In both cases, they studied the effect of the accretion rate on the GW amplitude and found that a higher accretion rate results in a larger GW amplitude. They also found that the frequency of the GW signal falls within the range of tens to hundreds of hertz, with the amplitude gradually decreasing as the frequency increases. Due to the requirement for extremely high accretion rates, Romero and colleagues concluded that GW signals from precessing accretion disks would likely only be detectable in the case of long GRBs. Based on the model of [80], Sun et al. (2012) calculated the GW signals from GRBs in the context of neutrino-dominated disk with disk-driven precession [150]. They found that the frequency of the resulting GW signals ranged from a few tenths of a hertz to tens of hertz, which was slightly lower than that predicted in the model proposed by [149]. Additionally, they found that the amplitude increased as the frequency rose, in contrast to the findings presented in [149]. For long GRBs occurring in local galaxies, the GWs could potentially be detected by GW detectors like DECIGO and the Big Bang Observer (BBO). Detecting GWs from GRBs would provide crucial insights into the dynamics of relativistic jets and the physics of their central engines.

6. Summary

Direct observational evidence for the jet precession of GRBs, including clearly periodic signals and QPOs in the prompt and afterglow light curves, has been actively sought. However, clearly periodic signals are always missing, while QPOs are rarely observed and are generally of poor quality. Therefore, it is suggested that in many cases, information in the GRB light curves related to jet precession could be encoded in a different way. Unfortunately, since several mechanisms can account for these non-periodic structures, it is not possible to definitively determine whether they are a consequence of jet precession. Beyond the morphology of the light curves, jet precession can also affect the ejecta structures, polarization signals, and GW signals. Jet precession can result in structured jets and depolarization of early optical afterglow polarization, and systems with precessing jets are capable of producing GW signals with prospects for their detection. Currently, although the effects of jet precession on various aspects of GRBs have been roughly understood theoretically, confirmation of the existence of precession in GRB jets remains a significant challenge due to the lack of direct or joint observations. In this scenario, simultaneous verification across multiple time phases (prompt and afterglow phases), multiple wavelengths (from radio to gamma rays), and even multiple aspects (e.g., jet structures, polarization, and GWs) is necessary. Fortunately, next-generation instruments show promise for providing additional clues in the search for evidence of GRB jet precession, for example, the Space-based multi-band astronomical Variable Objects Monitor (SVOM) with its capability for simultaneous multi-wavelength observations, including optical, X-ray, and gamma-ray bands, plus its ability to respond quickly, which should be able to detect afterglows much earlier, and high-quality QPOs caused by jet precession will be easier to detect, which is expected to assist in confirming the existence of jet precession in GRBs.

Funding: This work was supported by the National Key R&D Program of China under grant 2023YFA1607902, the National Natural Science Foundation of China under grants 12173031 and 12221003, and the China Postdoctoral Science Foundation under grant 2024M751769.

Conflicts of Interest: The authors declare no conflicts of interest.

References

1. Caproni, A.; Abraham, Z.; Monteiro, H. Parsec-scale jet precession in BL Lacertae (2200+420). *Mon. Not. R. Astron. Soc.* **2013**, *428*, 280–290. [CrossRef]
2. Qian, S.-J.; Britzen, S.; Witzel, A.; Krichbaum, T.P.; Gan, H.-Q.; Gao, L. A possible precessing nozzle and the Lense-Thirring effect in blazar 3C 454.3. *Res. Astron. Astrophys.* **2014**, *14*, 249–274. [CrossRef]
3. Caproni, A.; Abraham, Z.; Motter, J.C.; Monteiro, H. Jet precession driven by a supermassive black hole binary system in the BL Lac object PG 1553+113. *Astrophys. J. Lett.* **2017**, *851*, L39. [CrossRef]
4. Britzen, S.; Fendt, C.; Witzel, G.; Qian, S.-J.; Pashchenko, I.N.; Kurtanidze, O.; Zajacek, M.; Martinez, G.; Karas, V.; Aller, M.; et al. OJ287: Deciphering the 'Rosetta stone' of blazars. *Mon. Not. R. Astron. Soc.* **2018**, *478*, 3199–3219. [CrossRef]
5. Qian, S.J.; Britzen, S.; Witzel, A.; Krichbaum, T.P.; Kun, E. Model simulation of jet precession in quasar PG 1302–102. *Astron. Astrophys.* **2018**, *615*, A123. [CrossRef]
6. Britzen, S.; Zajaček, M.; Gopal-Krishna; Fendt, C.; Kun, E.; Jaron, F.; Sillanpää, A.; Eckart, A. Precession-induced Variability in AGN Jets and OJ 287. *Astrophys. J.* **2023**, *951*, 106. [CrossRef]
7. Caproni, A.; Mosquera Cuesta, H.J.; Abraham, Z. Observational Evidence of Spin-induced Precession in Active Galactic Nuclei. *Astrophys. J. Lett.* **2004**, *616*, L99–L102. [CrossRef]
8. Kudryavtseva, N.A.; Britzen, S.; Witzel, A.; Ros, E.; Karouzos, M.; Aller, M.F.; Aller, H.D.; Teräsranta, H.; Eckart, A.; Zensus, J.A. A possible jet precession in the periodic quasar B0605-085. *Astron. Astrophys.* **2011**, *526*, A51. [CrossRef]
9. Qian, S.J.; Britzen, S.; Witzel, A.; Krichbaum, T.P.; Gan, H.Q. Possible quasi-periodic ejections in quasar B1308+326. *Astron. Astrophys.* **2017**, *604*, A90. [CrossRef]
10. Britzen, S.; Fendt, C.; Zajaček, M.; Jaron, F.; Pashchenko, I.; Aller, M.F.; Aller, H.D. 3C 84: Observational Evidence for Precession and a Possible Relation to TeV Emission. *Galaxies* **2019**, *7*, 72. [CrossRef]
11. Nandi, S.; Caproni, A.; Kharb, P.; Sebastian, B.; Roy, R. Double-peaked Lines, Dual VLBI Components, and Precessing Jets in J1328+2752. *Astrophys. J.* **2021**, *908*, 178. [CrossRef]
12. Lobanov, A.P.; Roland, J. A supermassive binary black hole in the quasar 3C 345. *Astron. Astrophys.* **2005**, *431*, 831–846. [CrossRef]
13. Lu, J.-F.; Zhou, B.-Y. Observational Evidence of Jet Precession in Galactic Nuclei Caused by Accretion Disks. *Astrophys. J. Lett.* **2005**, *635*, L17–L20. [CrossRef]

14. Brown, R.L. Precessing jets in Sagittarius A: Gas dynamics in the central parsec of the galaxy. *Astrophys. J.* **1982**, *262*, 110–119. [CrossRef]
15. Romero, G.E.; Chajet, L.; Abraham, Z.; Fan, J.H. Beaming and precession in the inner jet of 3C 273 — II. The central engine. *Astron. Astrophys.* **2000**, *360*, 57–64.
16. Caproni, A.; Abraham, Z. Can long-term periodic variability and jet helicity in 3C 120 be explained by jet precession? *Mon. Not. R. Astron. Soc.* **2004**, *349*, 1218–1226. [CrossRef]
17. Caproni, A.; Abraham, Z. Precession in the Inner Jet of 3C 345. *Astrophys. J.* **2004**, *602*, 625–634. [CrossRef]
18. Martí-Vidal, I.; Marcaide, J.M.; Alberdi, A.; Pérez-Torres, M.A.; Ros, E.; Guirado, J.C. Detection of jet precession in the active nucleus of M 81. *Astron. Astrophys.* **2011**, *533*, A111. [CrossRef]
19. Gower, A.C.; Gregory, P.C.; Unruh, W.G.; Hutchings, J.B. Relativistic precessing jets in quasars and radio galaxies: Models to fit high resolution data. *Astrophys. J.* **1982**, *262*, 478–496. [CrossRef]
20. Ekers, R.D.; Fanti, R.; Lari, C.; Parma, P. NGC 326: A radio galaxy with a precessing beam. *Nature* **1978**, *276*, 588–590. [CrossRef]
21. Florido, E.; Battaner, E.; Sanchez-Saavedra, M.L. Spatial Distribution of Antisymmetrically Curved Extragalactic Radio Jets. *Astrophys. Space Sci.* **1990**, *164*, 131–137. [CrossRef]
22. Proctor, D.D. Morphological Annotations for Groups in the First Database. *Astrophys. J. Suppl. Ser.* **2011**, *194*, 31. [CrossRef]
23. Sethi, S.; Kuźmicz, A.; Jamrozy, M.; Slavcheva-Mihova, L. Discovery of a 100 kpc Narrow Curved Twin Jet in the S-shaped Giant Radio Galaxy J0644+1043. *Astrophys. J.* **2024**, *969*, 156. [CrossRef]
24. Pajdosz-Śmierciak, U.; Śmierciak, B.; Jamrozy, M. Possible jet reorientation in low-frequency radio structures of blazars. *Mon. Not. R. Astron. Soc.* **2022**, *514*, 2122–2134. [CrossRef]
25. Lense, J.; Thirring, H. Über den Einfluß der Eigenrotation der Zentralkörper auf die Bewegung der Planeten und Monde nach der Einsteinschen Gravitationstheorie. *Phys. Z.* **1918**, *19*, 156.
26. Bardeen, J.M.; Petterson, J.A. The Lense-Thirring Effect and Accretion Disks around Kerr Black Holes. *Astrophys. J. Lett.* **1975**, *195*, L65. [CrossRef]
27. Nealon, R.; Price, D.J.; Nixon, C.J. On the Bardeen-Petterson effect in black hole accretion discs. *Mon. Not. R. Astron. Soc.* **2015**, *448*, 1526–1540. [CrossRef]
28. Sarazin, C.L.; Begelman, M.C.; Hatchett, S.P. Disk-driven precession in SS 433. *Astrophys. J. Lett.* **1980**, *238*, L129–L132. [CrossRef]
29. Lu, J.F. Accretion disk-driven jet precession in active galactic nuclei. *Astron. Astrophys.* **1990**, *229*, 424–426.
30. Begelman, M.C.; Blandford, R.D.; Rees, M.J. Massive black hole binaries in active galactic nuclei. *Nature* **1980**, *287*, 307–309. [CrossRef]
31. Roos, N.; Kaastra, J.S.; Hummel, C.A. A massive binary black hole in 1928+738? *Astrophys. J.* **1993**, *409*, 130. [CrossRef]
32. Katz, J.I. A precessing disk in OJ 287? *Astrophys. J.* **1997**, *478*, 527. [CrossRef]
33. Britzen, S.; Roland, J.; Laskar, J.; Kokkotas, K.; Campbell, R.M.; Witzel, A. On the origin of compact radio sources. The binary black hole model applied to the gamma-bright quasar PKS 0420-014. *Astron. Astrophys.* **2001**, *374*, 784. [CrossRef]
34. Crampton, D.; Hutchings, J.B. The SS 433 binary system. *Astrophys. J.* **1981**, *251*, 604. [CrossRef]
35. Margon, B. Observations of SS 433. *Ann. Rev. Astron. Astrophys.* **1984**, *22*, 507. [CrossRef]
36. Fabrika, S. The jets and supercritical accretion disk in SS433. *Astrophys. Space Phys. Rev.* **2004**, *12*, 1. [CrossRef]
37. Veledina, A.; Poutanen, J.; Ingram, A. A unified Lense-Thirring precession model for optical and X-ray quasi-periodic oscillations in black hole binaries. *Astrophys. J.* **2013**, *778*, 165. [CrossRef]
38. de Ruiter, I.; van den Eijnden, J.; Ingram, A.; Uttley, P. A systematic study of the phase difference between QPO harmonics in black hole X-ray binaries. *Mon. Not. R. Astron. Soc.* **2019**, *485*, 3834–3844. [CrossRef]
39. Ma, X.; Tao, L.; Zhang, S.-N.; Zhang, L.; Bu, Q.-C.; Ge, M.-Y.; Chen, Y.-P.; Qu, J.-L.; Zhang, S.; Lu, F.-J.; et al. Discovery of oscillations above 200 keV in a black hole X-ray binary with Insight-HXMT. *Nat. Astron.* **2021**, *5*, 94–102. [CrossRef]
40. Meszaros, P. Gamma-ray bursts. *Rep. Prog. Phys.* **2006**, *69*, 2259–2321. [CrossRef]
41. Zhang, B. Gamma-Ray Bursts in the Swift Era. *Chin. J. Astron. Astrophys.* **2007**, *7*, 1–50. [CrossRef]
42. Kouveliotou, C.; Meegan, C.A.; Fishman, G.J.; Bhat, N.P.; Briggs, M.S.; Koshut, T.M.; Paciesas, W.S.; Pendleton, G.N. Identification of Two Classes of Gamma-Ray Bursts. *Astrophys. J. Lett.* **1993**, *413*, L101. [CrossRef]
43. Paciesas, W.S.; Meegan, C.A.; Pendleton, G.N.; Briggs, M.S.; Kouveliotou, C.; Koshut, T.M.; Lestrade, J.P.; McCollough, M.L.; Brainerd, J.J.; Hakkila, J.; et al. The Fourth BATSE Gamma-Ray Burst Catalog (Revised). *Astrophys. J. Suppl. Ser.* **1999**, *122*, 465–495. [CrossRef]
44. Stern, B.E.; Tikhomirova, Y.; Kompaneets, D.; Svensson, R.; Poutanen, J. An Off-Line Scan of the BATSE Daily Records and a Large Uniform Sample of Gamma-Ray Bursts. *Astrophys. J.* **2001**, *563*, 80–94. [CrossRef]
45. Zhang, B. Astrophysics: A burst of new ideas. *Nature* **2006**, *444*, 1010–1011. [CrossRef]
46. Nakar, E. Short-hard gamma-ray bursts. *Phys. Rep.* **2007**, *442*, 166–236. [CrossRef]
47. Abbott, B.P.; Abbott, R.; Abbott, T.D.; Acernese, F.; Ackley, K.; Adams, C.; Adams, T.; Addesso, P.; Adhikari, R.X.; Adya, V.B.; et al. Multi-messenger Observations of a Binary Neutron Star Merger. *Astrophys. J. Lett.* **2017**, *848*, L12. [CrossRef]
48. Abbott, B.P.; Abbott, R.; Abbott, T.D.; Acernese, F.; Ackley, K.; Adams, C.; Adams, T.; Addesso, P.; Adhikari, R.X.; Adya, V.B.; et al. Gravitational Waves and Gamma-Rays from a Binary Neutron Star Merger: GW170817 and GRB 170817A. *Astrophys. J. Lett.* **2017**, *848*, L13. [CrossRef]

49. Woosley, S.E.; Bloom, J.S. The Supernova Gamma-Ray Burst Connection. *Annu. Rev. Astron. Astrophys.* **2006**, *44*, 507–556. [CrossRef]
50. Woosley, S.E. Gamma-Ray Bursts from Stellar Mass Accretion Disks around Black Holes. *Astrophys. J.* **1993**, *405*, 273. [CrossRef]
51. Usov, V.V. Millisecond pulsars with extremely strong magnetic fields as a cosmological source of γ-ray bursts. *Nature* **1992**, *357*, 472–474. [CrossRef]
52. Dai, Z.G.; Lu, T. Gamma-ray burst afterglows and evolution of postburst fireballs with energy injection from strongly magnetic millisecond pulsars. *Astron. Astrophys.* **1998**, *333*, L87–L90. [CrossRef]
53. Zhang, B.; Mészáros, P. Gamma-Ray Burst Afterglow with Continuous Energy Injection: Signature of a Highly Magnetized Millisecond Pulsar. *Astrophys. J. Lett.* **2001**, *552*, L35–L38. [CrossRef]
54. Liu, T.; Gu, W.-M.; Zhang, B. Neutrino-dominated accretion flows as the central engine of gamma-ray bursts. *New Astron. Rev.* **2017**, *79*, 1–25. [CrossRef]
55. Blandford, R.D.; Znajek, R.L. Electromagnetic extraction of energy from Kerr black holes. *Mon. Not. R. Astron. Soc.* **1977**, *179*, 433–456. [CrossRef]
56. Rees, M.J.; Meszaros, P. Relativistic fireballs—Energy conversion and time-scales. *Mon. Not. R. Astron. Soc.* **1992**, *258*, 41. [CrossRef]
57. Meszaros, P.; Rees, M.J. Relativistic Fireballs and Their Impact on External Matter: Models for Cosmological Gamma-Ray Bursts. *Astrophys. J.* **1993**, *405*, 278. [CrossRef]
58. Rees, M.J.; Meszaros, P. Unsteady Outflow Models for Cosmological Gamma-Ray Bursts. *Astrophys. J. Lett.* **1994**, *430*, L93. [CrossRef]
59. Giannios, D. Prompt GRB emission from gradual energy dissipation. *Astron. Astrophys.* **2008**, *480*, 305–312. [CrossRef]
60. Beloborodov, A.M. Collisional mechanism for gamma-ray burst emission. *Mon. Not. R. Astron. Soc.* **2010**, *407*, 1033–1047. [CrossRef]
61. Zhang, B.; Yan, H. The Internal-collision-induced Magnetic Reconnection and Turbulence (ICMART) Model of Gamma-ray Bursts. *Astrophys. J.* **2011**, *726*, 90. [CrossRef]
62. Deng, M.; Schaefer, B.E. Search for millisecond periodic pulsations in BATSE gamma-ray bursts. *Astrophys. J.* **1997**, *491*, 720–724. [CrossRef]
63. Kruger, A.T.; Loredo, T.J.; Wasserman, I. Search for high-frequency periodicities in time-tagged event data from gamma-ray bursts and soft gamma repeaters. *Astrophys. J.* **2002**, *576*, 932–941. [CrossRef]
64. Dichiara, S.; Guidorzi, C.; Frontera, F.; Amati, L. A search for pulsations in short gamma-ray bursts to constrain their progenitors. *Astrophys. J.* **2013**, *777*, 132. [CrossRef]
65. Tarnopolski, M.; Marchenko, V. A comprehensive power spectral density analysis of astronomical time series. II. The Swift/BAT long gamma-ray bursts. *Astrophys. J.* **2021**, *911*, 20. [CrossRef]
66. Xiao, S.; Peng, W.-X.; Zhang, S.-N.; Xiong, S.-L.; Li, X.-B.; Tuo, Y.-L.; Gao, H.; Wang, Y.; Zheng, C.; Li, T.-P.; et al. Search for quasiperiodic oscillations in precursors of short and long gamma-ray bursts. *Astrophys. J.* **2022**, *941*, 166. [CrossRef]
67. Zhou, Z.-M.; Wang, X.-G.; Liang, E.-W.; Cao, J.-X.; Liu, H.-Y.; Li, C.-K.; Li, B.; Lin, D.-B.; Zheng, T.-C.; Lu, R.-J.; et al. A comprehensive analysis of Insight-HXMT gamma-ray burst data. I. Power density spectrum. *Astrophys. J.* **2024**, *972*, 190. [CrossRef]
68. Liu, D.-J.; Zou, Y.-C. Searching for QPOs in BATSE short gamma-ray bursts based on narrowband and broadband features. *J. Cosmol. Astropart. Phys.* **2024**, *2024*, 070. [CrossRef]
69. Chirenti, C.; Dichiara, S.; Lien, A.; Miller, M.C.; Preece, R. Kilohertz quasiperiodic oscillations in short gamma-ray bursts. *Nature* **2023**, *613*, 253–256. [CrossRef]
70. Xiao, S.; Zhang, Y.-Q.; Zhu, Z.-P.; Xiong, S.-L.; Gao, H. The peculiar precursor of a gamma-ray burst from a binary merger involving a magnetar. *Astrophys. J.* **2024**, *970*, 6. [CrossRef]
71. Chirenti, C.; Dichiara, S.; Lien, A.; Miller, M.C. Evidence of a strong 19.5 Hz flux oscillation in Swift BAT and Fermi GBM gamma-ray data from GRB 211211A. *Astrophys. J.* **2024**, *967*, 26. [CrossRef]
72. Blackman, E.G.; Yi, I.; Field, G.B. Relativistic precessing jets and cosmological gamma-ray bursts. *Astrophys. J. Lett.* **1996**, *473*, L79. [CrossRef]
73. Portegies Zwart, S.F.; Lee, C.-H.; Lee, H.K. Can precessing jets explain the light curves of gamma-ray bursts? *Astrophys. J.* **1999**, *520*, 666–679. [CrossRef]
74. Portegies Zwart, S.F.; Lee, C.-H.; Lee, H.K. Explaining the light curves of gamma-ray bursts with a precessing jet. *Astron. Astrophys. Suppl. Ser.* **1999**, *138*, 503–504. [CrossRef]
75. Portegies Zwart, S.F.; Totani, T. Precessing jets interacting with interstellar material as the origin for the light curves of gamma-ray bursts. *Mon. Not. R. Astron. Soc.* **2001**, *328*, 951–957. [CrossRef]
76. Stone, N.; Loeb, A.; Berger, E. Pulsations in short gamma ray bursts from black hole-neutron star mergers. *Phys. Rev. D* **2013**, *87*, 084053. [CrossRef]
77. Li, Y.; Shen, R.-F.; Zhang, B.-B. Quasiperiodic oscillation in short gamma-ray bursts from black hole-neutron star mergers. *Astrophys. J.* **2023**, *955*, 98. [CrossRef]
78. Reynoso, M.M.; Romero, G.E.; Sampayo, O.A. Precession of neutrino-cooled accretion disks in gamma-ray burst engines. *Astron. Astrophys.* **2006**, *454*, 11–16. [CrossRef]

79. Lei, W.H.; Wang, D.X.; Gong, B.P.; Huang, C.Y. A model of the light curves of gamma-ray bursts. *Astron. Astrophys.* **2007**, *468*, 563–569. [CrossRef]
80. Liu, T.; Liang, E.-W.; Gu, W.-M.; Zhao, X.-H.; Dai, Z.-G.; Lu, J.-F. Jet precession driven by neutrino-cooled disk for gamma-ray bursts. *Astron. Astrophys.* **2010**, *516*, A16. [CrossRef]
81. Wang, X.I.I.; Zhang, B.B.; Lei, W.H. GRB 200826A: A precursor of a long gamma-ray burst with missing main emission. *Astrophys. J. Lett.* **2022**, *931*, L2. [CrossRef]
82. Gao, H.; Li, A.; Lei, W.-H.; You, Z.-Q. Repeating emission episodes in gamma-ray bursts: Millilensing or jet precession? *Astrophys. J.* **2023**, *945*, 17. [CrossRef]
83. Zhang, Z.; Yin, Y.-H.; Wang, C.; Wang, X.; Yang, J.; Meng, Y.-Z.; Liu, Z.-K.; Chen, G.-Y.; Fu, X.; Gao, H.; et al. GRB 220408B: A three-episode burst from a precessing jet. *Res. Astron. Astrophys.* **2023**, *23*, 115023. [CrossRef]
84. Mészáros, P.; Rees, M.J. Optical and long-wavelength afterglow from gamma-ray bursts. *Astrophys. J.* **1997**, *476*, 232–237. [CrossRef]
85. LHAASO Collaboration; Cao, Z.; Aharonian, F.; An, Q.; Axikegu, A.; Bai, L.X.; Bai, Y.X.; Bao, Y.W.; Bastieri, D.; Bi, X.J.; et al. A tera-electron volt afterglow from a narrow jet in an extremely bright gamma-ray burst. *Science* **2023**, *380*, 1390–1396. [CrossRef]
86. Costa, E.; Frontera, F.; Heise, J.; Feroci, M.; in't Zand, J.; Fiore, F.; Cinti, M.N.; Dal Fiume, D.; Nicastro, L.; Orlandini, M.; et al. Discovery of an X-ray afterglow associated with the γ-ray burst of 28 February 1997. *Nature* **1997**, *387*, 783–785. [CrossRef]
87. Sari, R.; Piran, T.; Narayan, R. Spectra and light curves of gamma-ray burst afterglows. *Astrophys. J. Lett.* **1998**, *497*, L17–L20. [CrossRef]
88. Zhang, B.; Fan, Y.Z.; Dyks, J.; Kobayashi, S.; Mészáros, P.; Burrows, D.N.; Nousek, J.A.; Gehrels, N. Physical processes shaping gamma-ray burst X-ray afterglow light curves: Theoretical implications from the Swift X-ray telescope observations. *Astrophys. J.* **2006**, *642*, 354–370. [CrossRef]
89. Yi, S.-X.; Du, M.; Liu, T. Statistical analyses of the energies of X-ray plateaus and flares in gamma-ray bursts. *Astrophys. J.* **2022**, *924*, 69. [CrossRef]
90. Suvorov, A.G.; Kokkotas, K.D. Evidence for magnetar precession in X-ray afterglows of gamma-ray bursts. *Astrophys. J. Lett.* **2020**, *892*, L34. [CrossRef]
91. Suvorov, A.G.; Kokkotas, K.D. Precessing magnetars as central engines in short gamma-ray bursts. *Mon. Not. R. Astron. Soc.* **2021**, *502*, 2482–2494. [CrossRef]
92. Zou, L.; Zheng, T.-C.; Yang, X.; Zhang, H.-m.; Li, X.-Y.; Ren, J.; Lin, D.-B.; Liang, E.-W. GRB 101225A as orphan dipole radiation of a newborn magnetar with precession rotation in an off-axis gamma-ray burst. *Astrophys. J. Lett.* **2021**, *921*, L1. [CrossRef]
93. Zou, L.; Liang, E.-W. Early evolution of a newborn magnetar with strong precession motion in GRB 180620A. *Mon. Not. R. Astron. Soc.* **2022**, *513*, L89–L93. [CrossRef]
94. Zou, L.; Cheng, J.-G. Quasiperiodic oscillations in GRB 210514A: A case of a newborn supramassive precessing magnetar collapsing into a black hole? *Astrophys. J.* **2024**, *973*, 126. [CrossRef]
95. Zheng, T.-C.; Wei, D.-M.; Wang, Y.; Zhou, H.; Li, L. Black hole activity imprints on the internal plateau and the subsequent sharp decay. *Astrophys. J.* **2024**, *964*, 169. [CrossRef]
96. Hou, S.-J.; Liu, T.; Gu, W.-M.; Lin, D.-B.; Sun, M.-Y.; Wu, X.-F.; Lu, J.-F. Time evolution of flares in GRB 130925A: Jet precession in a black hole accretion system. *Astrophys. J.* **2014**, *781*, L19. [CrossRef]
97. Hou, S.-J.; Gao, H.; Liu, T.; Gu, W.-M.; Lin, D.-B.; Li, Y.-P.; Men, Y.-P.; Wu, X.-F.; Lei, W.-H.; Lu, J.-F. Variability of the giant X-ray bump in GRB 121027A and its possible origin. *Mon. Not. R. Astron. Soc.* **2014**, *441*, 2375–2379. [CrossRef]
98. Li, J.-D.; Gao, H.; Ai, S.; Lei, W.-H. Characteristics of gamma-ray burst afterglows in the context of non-axisymmetric structured jets. *Mon. Not. R. Astron. Soc.* **2023**, *525*, 6285–6294. [CrossRef]
99. Huang, B.-Q.; Liu, T. Energy injection driven by precessing jets in gamma-ray burst afterglows. *Astrophys. J.* **2021**, *916*, 71. [CrossRef]
100. Zhang, B. *The Physics of Gamma-Ray Bursts*, 1st ed.; Cambridge University Press: Cambridge, UK, 2018; pp. 663–664. [CrossRef]
101. Rhoads, J.E. How to tell a jet from a balloon: A proposed test for beaming in gamma-ray bursts. *Astrophys. J. Lett.* **1997**, *487*, L1–L4. [CrossRef]
102. Mészáros, P.; Rees, M.J.; Wijers, R.A.M.J. Viewing angle and environment effects in gamma-ray bursts: Sources of afterglow diversity. *Astrophys. J.* **1998**, *499*, 301–308. [CrossRef]
103. Lipunov, V.M.; Postnov, K.A.; Prokhorov, M.E. Gamma-ray bursts as standard-energy explosions. *Astron. Rep.* **2001**, *45*, 236–240. [CrossRef]
104. Rossi, E.; Lazzati, D.; Rees, M.J. Afterglow light curves, viewing angle and the jet structure of γ-ray bursts. *Mon. Not. R. Astron. Soc.* **2002**, *332*, 945–950. [CrossRef]
105. Zhang, B.; Mészáros, P. Gamma-Ray Burst Beaming: A Universal Configuration with a Standard Energy Reservoir? *Astrophys. J.* **2002**, *571*, 876–879. [CrossRef]
106. Zhang, B.; Dai, X.; Lloyd-Ronning, N.M.; Mészáros, P. Quasi-universal Gaussian Jets: A Unified Picture for Gamma-Ray Bursts and X-Ray Flashes. *Astrophys. J. Lett.* **2004**, *601*, L119–L122. [CrossRef]
107. Dai, X.; Zhang, B. A Global Test of a Quasi-universal Gamma-Ray Burst Jet Model through Monte Carlo Simulations. *Astrophys. J.* **2005**, *621*, 875–883. [CrossRef]

108. Frail, D.A.; Berger, E.; Galama, T.; Kulkarni, S.R.; Moriarty-Schieven, G.H.; Pooley, G.G.; Sari, R.; Shepherd, D.S.; Taylor, G.B.; Walter, F. The Enigmatic Radio Afterglow of GRB 991216. *Astrophys. J. Lett.* **2000**, *538*, L129–L132. [CrossRef]
109. Berger, E.; Kulkarni, S.R.; Pooley, G.; Frail, D.A.; McIntyre, V.; Wark, R.M.; Sari, R.; Soderberg, A.M.; Fox, D.W.; Yost, S.; et al. A common origin for cosmic explosions inferred from calorimetry of GRB030329. *Nature* **2003**, *426*, 154–157. [CrossRef]
110. Abbott, B.P.; Abbott, R.; Abbott, T.D.; Acernese, F.; Ackley, K.; Adams, C.; Adams, T.; Addesso, P.; Adhikari, R.X.; Adya, V.B.; et al. GW170817: Observation of Gravitational Waves from a Binary Neutron Star Inspiral. *Phys. Rev. Lett.* **2017**, *119*, 161101. [CrossRef]
111. Troja, E.; Piro, L.; van Eerten, H.; Wollaeger, R.T.; Im, M.; Fox, O.D.; Butler, N.R.; Cenko, S.B.; Sakamoto, T.; Fryer, C.L.; et al. The X-ray counterpart to the gravitational-wave event GW170817. *Nature* **2017**, *551*, 71–74. [CrossRef]
112. Troja, E.; Piro, L.; Ryan, G.; van Eerten, H.; Ricci, R.; Wieringa, M.H.; Lotti, S.; Sakamoto, T.; Cenko, S.B. The outflow structure of GW170817 from late-time broad-band observations. *Mon. Not. R. Astron. Soc.* **2018**, *478*, L18–L23. [CrossRef]
113. Urrutia, G.; De Colle, F.; Murguia-Berthier, A.; Ramirez-Ruiz, E. What determines the structure of short gamma-ray burst jets? *Mon. Not. R. Astron. Soc.* **2021**, *503*, 4363–4371. [CrossRef]
114. Nativi, L.; Lamb, G.P.; Rosswog, S.; Lundman, C.; Kowal, G. Are interactions with neutron star merger winds shaping the jets? *Mon. Not. R. Astron. Soc.* **2022**, *509*, 903–913. [CrossRef]
115. Urrutia, G.; De Colle, F.; López-Cámara, D. Three-dimensional numerical simulations of structured gamma-ray burst jets. *Mon. Not. R. Astron. Soc.* **2023**, *518*, 5145–5153. [CrossRef]
116. Zhang, W.; Woosley, S.E.; MacFadyen, A.I. Relativistic jets in collapsars. *Astrophys. J.* **2003**, *586*, 356–371. [CrossRef]
117. Huang, B.-Q.; Lin, D.-B.; Liu, T.; Ren, J.; Wang, X.-G.; Liu, H.-B.; Liang, E.-W. Jet structure in the afterglow phase for gamma-ray bursts with a precessing jet. *Mon. Not. R. Astron. Soc.* **2019**, *487*, 3214–3220. [CrossRef]
118. Birnholtz, O.; Piran, T. Gravitational wave memory from gamma ray bursts' jets. *Phys. Rev. D* **2013**, *87*, 123007. [CrossRef]
119. Sago, N.; Ioka, K.; Nakamura, T.; Yamazaki, R. Gravitational wave memory of gamma-ray burst jets. *Phys. Rev. D* **2004**, *70*, 104012. [CrossRef]
120. Akiba, S.; Nakada, M.; Yamaguchi, C.; Iwamoto, K. Gravitational-Wave Memory from the Relativistic Jet of Gamma-Ray Bursts. *Publ. Astron. Soc. Jpn.* **2013**, *65*, 59. [CrossRef]
121. Huang, B.-Q.; Liu, T.; Xue, L.; Qi, Y.-Q. Low-frequency Gravitational-wave Memories from Gamma-Ray Burst Afterglows with Energy Injections. *Astrophys. J.* **2023**, *944*, 189. [CrossRef]
122. Willis, D.R.; Barlow, E.J.; Bird, A.J.; Clark, D.J.; Dean, A.J.; McConnell, M.L.; Moran, L.; Shaw, S.E.; Sguera, V. Evidence of polarisation in the prompt gamma-ray emission from GRB 930131 and GRB 960924. *Astron. Astrophys.* **2005**, *439*, 245–253. [CrossRef]
123. McGlynn, S.; Clark, D.J.; Dean, A.J.; Hanlon, L.; McBreen, S.; Willis, D.R.; McBreen, B.; Bird, A.J.; Foley, S. Polarisation studies of the prompt gamma-ray emission from GRB 041219a using the spectrometer aboard INTEGRAL. *Astron. Astrophys.* **2007**, *466*, 895–904. [CrossRef]
124. Sharma, V.; Iyyani, S.; Bhattacharya, D.; Chattopadhyay, T.; Rao, A.R.; Aarthy, E.; Vadawale, S.V.; Mithun, N.P.S.; Bhalerao, V.B.; Ryde, F.; et al. Time-varying Polarized Gamma-Rays from GRB 160821A: Evidence for Ordered Magnetic Fields. *Astrophys. J. Lett.* **2019**, *882*, L10. [CrossRef]
125. Gupta, R.; Gupta, S.; Chattopadhyay, T.; Lipunov, V.; Castro-Tirado, A.J.; Bhattacharya, D.; Pandey, S.B.; Oates, S.R.; Kumar, A.; Hu, Y.D.; et al. Probing into emission mechanisms of GRB 190530A using time-resolved spectra and polarization studies: Synchrotron origin? *Mon. Not. R. Astron. Soc.* **2022**, *511*, 1694–1713. [CrossRef]
126. Zhang, S.-N.; Kole, M.; Bao, T.-W.; Batsch, T.; Bernasconi, T.; Cadoux, F.; Chai, J.-Y.; Dai, Z.-G.; Dong, Y.-W.; Gauvin, N.; et al. Detailed polarization measurements of the prompt emission of five gamma-ray bursts. *Nat. Astron.* **2019**, *3*, 258–264. [CrossRef]
127. Mundell, C.G.; Steele, I.A.; Smith, R.J.; Kobayashi, S.; Melandri, A.; Guidorzi, C.; Gomboc, A.; Mottram, C.J.; Clarke, D.; Monfardini, A.; et al. Early optical polarization of a gamma-ray burst afterglow. *Science* **2007**, *315*, 1822. [CrossRef]
128. Steele, I.A.; Mundell, C.G.; Smith, R.J.; Kobayashi, S.; Guidorzi, C. Ten per cent polarized optical emission from GRB090102. *Nature* **2009**, *462*, 767–769. [CrossRef]
129. Uehara, T.; Toma, K.; Kawabata, K.S.; Chiyonobu, S.; Fukazawa, Y.; Ikejiri, Y.; Inoue, T.; Itoh, R.; Komatsu, T.; Miyamoto, H.; et al. GRB 091208B: First detection of the optical polarization in early forward shock emission of a gamma-ray burst afterglow. *Astrophys. J. Lett.* **2012**, *752*, L6. [CrossRef]
130. Mundell, C.G.; Kopač, D.; Arnold, D.M.; Steele, I.A.; Gomboc, A.; Kobayashi, S.; Harrison, R.M.; Smith, R.J.; Guidorzi, C.; Virgili, F.J.; et al. Highly polarized light from stable ordered magnetic fields in GRB 120308A. *Nature* **2013**, *504*, 119–121. [CrossRef]
131. Kopač, D.; Mundell, C.G.; Japelj, J.; Arnold, D.M.; Steele, I.A.; Guidorzi, C.; Dichiara, S.; Kobayashi, S.; Gomboc, A.; Harrison, R.M.; et al. Limits on optical polarization during the prompt phase of GRB 140430A. *Astrophys. J.* **2015**, *813*, 1. [CrossRef]
132. Steele, I.A.; Kopač, D.; Arnold, D.M.; Smith, R.J.; Kobayashi, S.; Jermak, H.E.; Mundell, C.G.; Gomboc, A.; Guidorzi, C.; Melandri, A.; et al. Polarimetry and photometry of gamma-ray bursts with RINGO2. *Astrophys. J.* **2017**, *843*, 143. [CrossRef]
133. Jordana-Mitjans, N.; Mundell, C.G.; Smith, R.J.; Guidorzi, C.; Marongiu, M.; Kobayashi, S.; Gomboc, A.; Shrestha, M.; Steele, I.A. Coherence scale of magnetic fields generated in early-time forward shocks of GRBs. *Mon. Not. R. Astron. Soc.* **2021**, *505*, 2662–2674. [CrossRef]
134. Shrestha, M.; Steele, I.A.; Kobayashi, S.; Smith, R.J.; Guidorzi, C.; Jordana-Mitjans, N.; Jermak, H.; Arnold, D.; Mundell, C.G.; Gomboc, A. Polarimetry and photometry of gamma-ray bursts afterglows with RINGO3. *Mon. Not. R. Astron. Soc.* **2022**, *516*, 1584–1600. [CrossRef]

135. Wijers, R.A.M.J.; Vreeswijk, P.M.; Galama, T.J.; Rol, E.; van Paradijs, J.; Kouveliotou, C.; Giblin, T.; Masetti, N.; Palazzi, E.; Pian, E.; et al. Detection of Polarization in the Afterglow of GRB 990510 with the ESO Very Large Telescope. *Astrophys. J.* **1999**, *523*, L33–L36. [CrossRef]
136. Hjorth, J.; Bjornsson, G.; Andersen, M.I.; Caon, N.; Cairos, L.M.; Castro-Tirado, A.J.; Zapatero Osorio, M.R.; Pedersen, H.; Costa, E. Polarimetric constraints on the optical afterglow emission from GRB 990123. *Science* **1999**, *283*, 2073. [CrossRef]
137. Rol, E.; Wijers, R.A.M.J.; Vreeswijk, P.M.; Kaper, L.; Galama, T.J.; van Paradijs, J.; Kouveliotou, C.; Masetti, N.; Pian, E.; Palazzi, E.; et al. GRB 990712: First indication of polarization variability in a gamma-ray burst afterglow. *Astrophys. J.* **2000**, *544*, 707. [CrossRef]
138. Masetti, N.; Palazzi, E.; Pian, E.; Simoncelli, A.; Hunt, L.K.; Maiorano, E.; Levan, A.; Christensen, L.; Rol, E.; Savaglio, S.; et al. Optical and near-infrared observations of the GRB020405 afterglow. *Astron. Astrophys.* **2003**, *404*, 465–481. [CrossRef]
139. Barth, A.J.; Sari, R.; Cohen, M.H.; Goodrich, R.W.; Price, P.A.; Fox, D.W.; Bloom, J.S.; Soderberg, A.M.; Kulkarni, S.R. Optical spectropolarimetry of the GRB 020813 afterglow. *Astrophys. J. Lett.* **2003**, *584*, L47. [CrossRef]
140. Rol, E.; Wijers, R.A.M.J.; Fynbo, J.P.U.; Hjorth, J.; Gorosabel, J.; Egholm, M.P.; Castro Cerón, J.M.; Castro-Tirado, A.J.; Kaper, L.; Masetti, N.; et al. Variable polarization in the optical afterglow of GRB 021004. *Astron. Astrophys.* **2003**, *405*, L23–L27.:20030731 [CrossRef]
141. Maiorano, E.; Masetti, N.; Palazzi, E.; Savaglio, S.; Rol, E.; Vreeswijk, P.M.; Pian, E.; Price, P.A.; Peterson, B.A.; Jelínek, M.; et al. Physics of the GRB 030328 afterglow and its environment. *Astron. Astrophys.* **2006**, *455*, 423–431.:20054728 [CrossRef]
142. Wiersema, K.; Curran, P.A.; Krühler, T.; Melandri, A.; Rol, E.; Starling, R.L.C.; Tanvir, N.R.; van der Horst, A.J.; Covino, S.; Fynbo, J.P.U.; et al. Detailed optical and near-infrared polarimetry, spectroscopy and broad-band photometry of the afterglow of GRB 091018: Polarization evolution. *Mon. Not. R. Astron. Soc.* **2012**, *426*, 2–22. [CrossRef]
143. Granot, J.; Königl, A. Linear polarization in gamma-ray bursts: The case for an ordered magnetic field. *Astrophys. J. Lett.* **2003**, *594*, L83–L87. [CrossRef]
144. Lan, M.-X.; Xue, R.; Xiong, D.; Lei, W.-H.; Wu, X.-F.; Dai, Z.-G. Polarization of astrophysical events with precessing jets. *Astrophys. J.* **2019**, *878*, 140. [CrossRef]
145. Huang, B.-Q.; Liu, T. Polarization in early optical afterglows of gamma-ray bursts driven by precessing jets. *Astrophys. J.* **2022**, *933*, 103. [CrossRef]
146. Abbott, B.P.; Abbott, R.; Abbott, T.D.; Abernathy, M.R.; Acernese, F.; Ackley, K.; Adams, C.; Adams, T.; Addesso, P.; Adhikari, R.X.; et al. Properties of the Binary Black Hole Merger GW150914. *Phys. Rev. Lett.* **2016**, *116*, 241102. [CrossRef]
147. Segalis, E.B.; Ori, A. Emission of gravitational radiation from ultrarelativistic sources. *Phys. Rev. D* **2001**, *64*, 064018. [CrossRef]
148. Yu, Y.-W. Gravitational-wave Memory from a Propagating Relativistic Jet: A Probe of the Interior of Gamma-Ray Burst Progenitors. *Astrophys. J.* **2020**, *897*, 19. [CrossRef]
149. Romero, G.E.; Reynoso, M.M.; Christiansen, H.R. Gravitational radiation from precessing accretion disks in gamma-ray bursts. *Astron. Astrophys.* **2010**, *524*, A4. [CrossRef]
150. Sun, M.-Y.; Liu, T.; Gu, W.-M.; Lu, J.-F. Gravitational Waves of Jet Precession in Gamma-Ray Bursts. *Astrophys. J.* **2012**, *752*, 31. [CrossRef]